Understanding Hybrid Lipid-Polymer Gene Delivery Nanoparticle Assembly with Fluorescence Cross Correlation Spectroscopy

Juan L. Paris[1,*], Ricardo Gaspar[1], Filipe Coelho[1], Pieter A. A. De Beule[1], Bruno F. B. Silva[1,*]

[1]International Iberian Nanotechnology Laboratory, Av. Mestre José Veiga, Braga, Portugal

*Corresponding authors: juan.paris@ibima.eu, bruno.silva@inl.int

Abstract: Hybrid lipid-polymer-nucleic acid nanoparticles (LPNPs) provide a range of delivery strategies for nonviral gene therapy. However, due to several pairwise interactions between their components, these formulations are difficult to predict and characterize. Here, we employed, for the first time, a novel methodology based on fluorescence cross correlation spectroscopy (FCCS) to directly quantify the extent of association between polycation-DNA cores (polyplexes) and cationic liposome shells. This leads to a rapid and easy evaluation of LPNP formation. As a result, we were able to unveil two critical insights for predicting LPNP assembly. Firstly, the interaction between the polycation (polylysine) and DNA is robust, with the polycation not being displaced by liposomes. Hence, the polyplex cores and liposome shells have to be oppositely charged to associate. Secondly, and most importantly, the liposome:poliplex number ratio (ρ_N), as opposed to the more common charge ratio, is a critical parameter to predict stable LPNP formation. We find that $\rho_N \geq 1$ is required to ensure that every polyplex is enveloped by a liposome, avoiding the coexistence of oppositely charged species, thus inhibiting aggregation. Since the chosen LPNP components are common, these observations should be applicable to many LPNP systems. Furthermore, this FCCS-based methodology is relevant to other self-assembly composite materials, for applications beyond gene delivery.

Keywords: Lipopolyplex, Lipid-polycation-DNA (LPD), gene delivery, fluorescence cross-correlation spectroscopy, FCCS.

1. INTRODUCTION

The relevance of non-viral gene delivery to treat genetic and acquired diseases has become evident with the first FDA-approved treatment using siRNA for hereditary transthyretin-mediated amyloidosis[1] and the recent success of lipid-based mRNA vaccines to address the Coronavirus disease (COVID-19) pandemic[2,3]. New applications of the technology encompass also the development of personalized cancer vaccines[4–6] and permanent knockout of defective genes using the CRISPR/Cas9 platform[7], which start showing exciting early-stage clinical trial results. Despite these leaps forward, the efficacy of non-viral gene therapies is still limited in many cases, particularly for therapeutic targets beyond the liver and immune cells[8,9]. This motivates the study of new delivery systems capable of overcoming the many

hurdles that nucleic acid-carrying nanosystems must overcome to efficiently deliver genes in patients[10–14].

Nucleic acids (NAs) such as DNA and mRNA are highly negatively charged molecules that for most gene delivery applications need to be compacted and encapsulated into a nanocarrier. This is efficiently done using oppositely charged species such as cationic lipids and polymers (i.e., polycations), which interact strongly via electrostatic interactions with NAs to form macroscopic or nanosized complexes in an entropy-driven process[10,15–17]. NA complexes using cationic lipids are often designated by lipoplexes or lipid nanoparticles (LNPs)[17,18], whereas those using polycations are usually designated by polyplexes[10]. Nucleic acid LNPs containing ionizable lipids have recently gained momentum as FDA-approved efficient delivery systems[1,19–21]. Yet, more formulations and nano-architectures are needed for a wider array of therapeutic strategies.

A particularly interesting architecture consists of a polyplex core composed by polycations complexed with nucleic acids, enveloped by a lipid membrane (Figure 1a)[22–25]. Such hybrid lipid-polycation-nucleic acid nanoparticles (LPNPs) are also often referred to by lipopolyplexes. These formulations are more complex, but their core and shell components can be independently designed to act sequentially[22], for example through a cell type-targeted outer lipid membrane and a polycation core optimized for endosomal escape[26]. In addition, LPNPs allow using cationic[27–30], anionic[31,32], or neutral lipid membranes[33] as the outer shell, which is not easily achieved using lipid-NA lipoplexes. Moreover, depending on the method of assembly, the lipid membranes can be constituted either by bilayers[27–33] or monolayers[34–37]. This significantly expands the available options for nanocarrier design, drawing attention both from academic and industrial research[25,38].

However, because of the three components used in LPNPs, more pair-wise interactions (polycation-DNA, liposome-DNA and liposome-polycation) need to be considered, making the formulations also more complex to predict and characterize. This is particularly important when a bilayer is to be added, which typically involves charged liposomes. Typically, to form a core polyplex enveloped by a lipid bilayer, the polyplex core is assembled in a first step, followed by the addition of oppositely charged liposomes to drive the electrostatic complexation between both species. This is reminiscent of the widely used electrostatic-based layer-by-layer assembly[39,40].

If the polycation and cationic lipids are added to the nucleic acids at the same time, alternative structures to the core-shell LPNPs may form[25,41]. However, even when the polyplex core is formed earlier and the lipid membrane added after, competing interactions between the tree components can still, at least in

principle, drive the formation of other structures and displace one of the components (Figure 1a). This is found, for instance, when heparin (a strong polyanion) is added to lipoplexes, resulting in the displacement of DNA from the liposomes[42] instead of forming a polymer shell around the lipoplex. This makes routine characterization of LPNPs challenging as it is difficult to assess if liposomes are effectively associating with the polyplex cores, as intended, or if other elusive processes are taking place.

Here we propose an approach based on dual colour Fluorescence Cross-Correlation Spectroscopy (FCCS) to quantitatively assess the extent of association between polyplexes and liposomes in the formation of LPNPs. By analysing the extent of correlation between the fluorescence intensity fluctuations of two labelled species as they diffuse in-and-out of a confocal volume (Figure 2a), the colocalization/association between them can be quantified [43–45], providing a way to obtain crucial insights about the assembly of LPNPs. Overall, we show that the formation of colloidally-stable nanoparticles containing the three components (polylysine, DNA and liposomes) can be achieved in a regime where polyplexes are initially negative and their charge is inverted to positive by addition of cationic liposomes. However, the crucial parameter to obtain colloidal stability is not the overall molar charge ratio, but rather the ratio between the numbers of cationic liposomes and anionic polyplexes, provided that each liposome has a higher absolute charge than the polyplexes. This quantity is elusive to determine based only on the composition of the systems but is easily accessed with FCCS. Besides elucidating the general assembly behaviour of LPNP systems, this approach is likely to be of interest to other composite materials involving hierarchical assembly.

2. RESULTS AND DISCUSSION

2.1. Size and ζ potential reveal stability regions and hint at LPNP formation.

To investigate the assembly behaviour of hybrid lipid-polycation-DNA nanoparticles (LPNPs), a series of samples with varying ratios between the three components was prepared. As DNA is the only anionic component, and both the liposomes and polycations are cationic, it is convenient to define the sample compositions by the ratios of both the cationic lipids in the liposomes to anionic groups (phosphate) in DNA, which we define as $\rho_{\mathrm{L:DNA}}$, and by the ratio of ionizable-cationic amine groups in the polycations to anionic groups in DNA, which we define as $\rho_{\mathrm{P:DNA}}$. To make these results as general as possible, polylysine (PLL), a very generic cationic polymer in both polyplex and LPNP systems[31,46,47], was chosen as the polycation. For the cationic liposome a generic DOTAP:DOPC:PEG2K formulation was used, with fixed amount (80 mol%) of the cationic lipid DOTAP and varying amounts of PEG-lipid. Together with

the concentration of PLL, which was fixed at 7 μg/ml, $\rho_{L:DNA}$ and $\rho_{P:DNA}$ fully define the system composition.

The strategy for assembling LPNPs is shown in Figure 1a. Briefly, the polyplex core is assembled in a preliminary step by mixing PLL with DNA at a fixed $\rho_{P:DNA}$ ratio. On a second step, the cationic liposomes are added to form the core-shell LPNPs. The isoelectric point (ρ_{iso}) between PLL and DNA was determined at 1.6[48]. To have a suitable range of LPNP compositions to rationalize the general assembly behaviour, three starting polyplex $\rho_{P:DNA}$ ratios were selected: 1, 1.5 and 3. Their ζ potential and hydrodynamic diameter (D_H) can be seen in Figures 1b and 1c and Table S1.

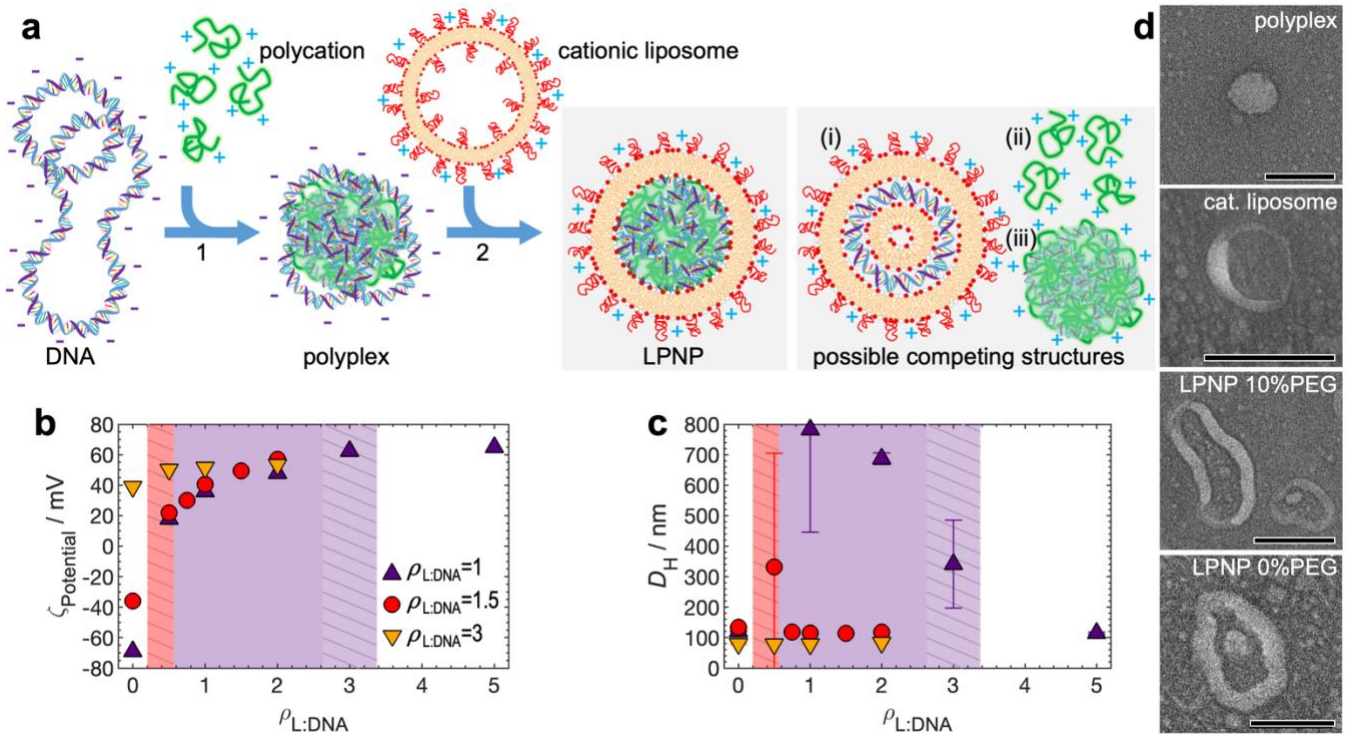

Figure 1. Lipid-Polymer hybrid nanoparticle (LPNP) assembly and physical properties. (**a**) Schematic illustration of the LPNP assembly strategy, consisting of a preliminary step (1) where DNA and polycations are mixed to form polyplexes with an excess negative charge, and a second step (2) where polyplexes are mixed with oppositely charged cationic liposomes to form LPNPs. Along with (or instead of) LPNP formation, hypothetical competing structures can form, such as lipid-DNA complexes (i), polycations released from the polyplex core (ii) or positively charged polyplexes striped from the outer DNA layers (iii). (**b**) ζ potential and (**c**) hydrodynamic diameter (D_H) of the three LPNP systems as a function of $\rho_{L:DNA}$. The red dashed area represents the region of the $\rho_{P:DNA}$=1.5 system where aggregation was observed in some samples. The purple area represents the region of the $\rho_{P:DNA}$=1 system where large aggregation was observed, and the purple dashed area represents the region where aggregation was observed only in some samples. Data are Means ± SD (n=3). (**d**) TEM images of polyplexes, liposomes and LPNPs with 10 and 0 mol% PEG.

For $\rho_{P:DNA}$=1, the polyplexes are negatively overcharged with DNA, showing a negative ζ potential (Figure 1b) and are likely to contain also a significant fraction of non-complexed DNA in excess[46]. For $\rho_{P:DNA}$=1.5, the polyplexes are still negatively charged, although to a smaller extent than for $\rho_{P:DNA}$=1. Given the proximity with ρ_{iso} , these polyplexes are likely to contain just a minute amount of non-complexed DNA, if any. For $\rho_{P:DNA}$=3, the polyplexes are positively charged, and virtually all the DNA is expected to be complexed and coexisting with non-complexed polycation in excess. The size of the obtained polyplexes varies also as a function of $\rho_{P:DNA}$, being all smaller than 150 nm, and with $\rho_{P:DNA}$=3 showing the smallest diameter (<80 nm). The prepared cationic liposomes presented a diameter of ca. 100 nm and very high ζ potential values (Table S2).

For the formation of LPNPs, different amounts of cationic liposomes with 10 mol% PEGylated lipid were added to the different Polyplexes. Figure 1b-1c shows the ζ potential and size results for the LPNP formulations as a function of $\rho_{L:DNA}$ for the three different starting polyplexes. The complete set of data including D_H, polydispersity index (PDI) and ζ potential can be found in Table S3.

The results in Figure 1b-1c show two different trends for the LPNP systems depending on the surface charge of the starting polyplex. For samples obtained from cationic polyplexes ($\rho_{P:DNA}$=3), neither the size nor the ζ potential were significantly affected when different amounts of cationic liposomes were added. Conversely, when the starting polyplex presents negative ζ potential ($\rho_{P:DNA}$=1 and 1.5), the LPNP charge switched to cationic already at the lowest $\rho_{L:DNA}$ additions, coinciding also with the observation of strong aggregation (D_H>500 nm), especially for $\rho_{P:DNA}$=1. Further addition of liposomes led to stabilization of the systems. Marginal stability for $\rho_{P:DNA}$=1 and $\rho_{P:DNA}$=1.5 LPNPs is reached at $\rho_{L:DNA}$=3 and $\rho_{L:DNA}$=0.5, respectively, since aggregation was observed only in some batches. Clear solutions with D_H<120 nm were obtained for $\rho_{L:DNA}$=5 and $\rho_{L:DNA}$≥0.75 for $\rho_{P:DNA}$=1 and $\rho_{P:DNA}$=1.5 LPNPs, respectively. Since $\rho_{P:DNA}$=1 polyplexes are more negatively charged and are expected to coexist with a significant amount of free DNA in solution (which needs to be neutralized), more liposomes are needed to stabilize these LPNPs when compared with the $\rho_{P:DNA}$=1.5 system. Yet, at a first glance, the factor of ca. six times larger $\rho_{L:DNA}$ needed to stabilize $\rho_{P:DNA}$=1 polyplexes seems high. TEM results (Figure 1d) confirm the formation of LPNPs, with imaged particles showing a core similar to the polyplex samples, enveloped by a membrane.

Altogether, the observation that negative polyplexes first aggregate and then redisperse as $\rho_{L:DNA}$ is increased hints at strong electrostatic interactions with liposomes and to the conversion of polyplexes into LPNPs. However, one should consider also other potential interactions leading to the formation of competing structures instead of LPNPs (Figure 1a). For instance, DNA could be partially or entirely

displaced from the polycation to the cationic liposomes to form lipoplexes. Such structures could have sizes and ζ potential like LPNPs. Regarding the positively charged polyplexes ($\rho_{P:DNA}$=3), the lack of observable changes with $\rho_{L:DNA}$ could hint at no formation of LPNPs, but also here one should consider the possibility of cationic liposomes displacing some polycations to form LPNPs. These alternative scenarios are difficult to discern with DLS/electrophoretic mobility and even with TEM, since the samples are dried and it is difficult to probe large sample areas.

2.2. Dual-colour fluorescence time traces provide semi-quantitative colocalization between cationic liposomes and polyplexes.

The colocalization between two species labelled with two distinct fluorophores can be assessed qualitatively by looking at the spatial overlap between the two labels using fluorescence microscopy[33]. However, this approach is challenging to render quantitative[49]. FCCS can overcome this limitation and provide a quantitative measure of colocalization along with simultaneous determination of the sizes of the labelled species[43,44]. FCCS has been successfully used to characterize interactions between biologic species such as proteins, nucleic acids and membranes, including in living cells[43,44,50–52]. In the context of nanoparticle characterization, FCCS has been employed to monitor the release of nucleic acids from lipoplexes[53], and to assess the formation of polymeric[54] and silica nanoparticles[55,56], lipid bilayer-coated metal organic frameworks[57], and cationic liposome-DNA complexes[45,58].

To monitor the formation of LPNPs (illustrated in Figure 1a), we covalently-label PLL with Atto-488 (green) and the cationic liposomes with Texas-Red. Since the two labelled species are cationic, they can only associate if DNA acts as an intermediary. Hence, the colocalization between PLL and liposomes indicates that liposomes have associated with the polyplex core. Simultaneously, this rules out other competing structures in which DNA would be displaced, as illustrated in Figure 1a. If DNA was to be labelled instead of polycations, the absence of cross-correlation between the two signals would still discard the formation of LPNPs, but its presence would not allow the distinction between LPNPs or other competing structures (e.g., lipoplexes). In the case of formulations starting with cationic polyplexes ($\rho_{P:DNA}$=3), the existence of labelled polycation free in solution makes the FCCS measurements difficult to analyse, and in this case the initial measurements were complemented with measurements in which the DNA is labelled (YOYO-1, green) instead of the polycation.

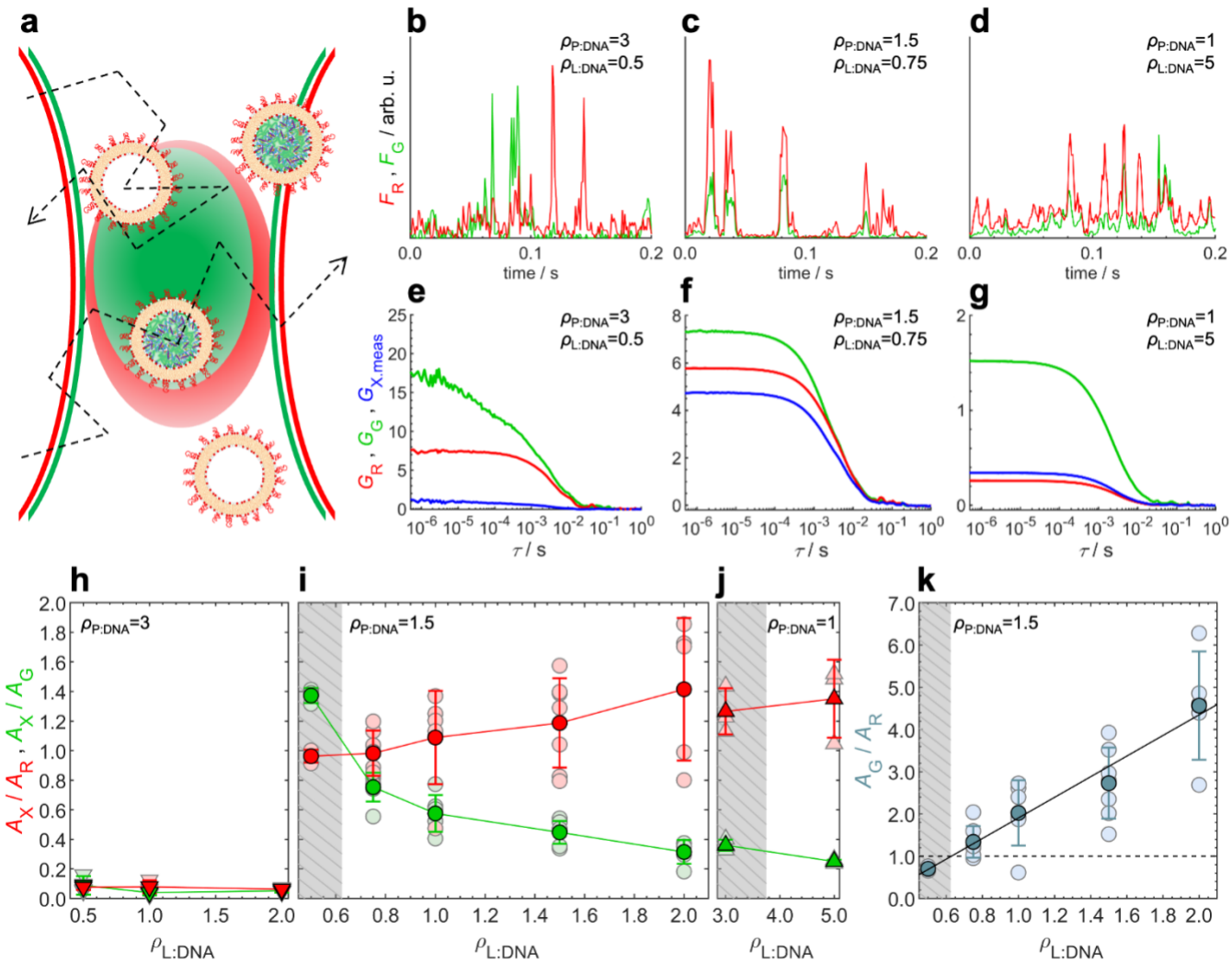

Figure 2. FCCS quantifies association between cationic liposomes and polyplexes. (**a**) Schematic illustration of the green and red confocal volumes with LPNPs and cationic liposomes diffusing through them. Panels **b**-**d** show representative fluorescence time traces for samples $\rho_{P:DNA}$=3, $\rho_{L:DNA}$=0.5; $\rho_{P:DNA}$=1.5, $\rho_{L:DNA}$=0.75; and $\rho_{P:DNA}$=1, $\rho_{L:DNA}$=5, respectively. Panels **e**-**g** show the corresponding auto and cross-correlation curves for the same samples. The green and red fluorescence (F_G and F_R) and auto-correlation curves (G_G and G_R) are shown in green and red, respectively. The cross-correlation curves ($G_{X.meas}$) are shown in blue. Non-associating particles, like cationic polyplexes and cationic liposomes, diffuse independently, producing uncorrelated green and red fluorescence fluctuations, visible both in the time traces (**b**) and in the negligeable amplitude of $G_{X.meas}$. in (**e**). LPNPs, containing both a polyplex (labelled with Atto488, green) and a cationic liposome (Texas-Red) produce correlated green and red fluorescence fluctuations, visible both in the time traces (**c** and **d**), and large amplitudes of $G_{X.meas}$ (**f** and **g**). Panels **h**-**j**, show the A_X/A_R (red symbols) and A_X/A_G (green symbols) ratios, which provide the fraction of polyplexes converted to LPNPs and the fraction of liposomes used in LPNPs, respectively. A_X/A_R and A_X/A_G are very low for the $\rho_{P:DNA}$=3 system, confirming negligeable association between polyplexes and liposomes with the same charge sign (**h**). The A_X/A_R ratio for $\rho_{P:DNA}$=1.5 (**i**) and $\rho_{P:DNA}$=1 (**j**) systems is ≈1 for low $\rho_{L:DNA}$ and increases slightly as $\rho_{L:DNA}$ increases, indicating full conversion of polyplexes to LPNPs, and an average number of liposomes per LPNP increasing slightly beyond one with $\rho_{L:DNA}$. Conversely, A_X/A_G decreases steadily with $\rho_{L:DNA}$, indicating that after colloidal stability is reached, most added liposomes are in excess, not associating with LPNPs. Panel **k** shows the A_G/A_R ratio (for $\rho_{P:DNA}$=1.5), which is equivalent to the liposome:polyplex ratio (ρ_N) . The

region of robust colloidal stability for LPNPs shows ρ_N>1. The region of marginal stability shows ρ_N<1. This suggests that $\rho_N \geq 1$ is a requirement for robust stability. The boundary between marginal and robust stability (ρ_N=1) is estimated at $\rho_{L:DNA}$=0.63 for $\rho_{P:DNA}$=1.5. The grey-dashed areas in **h-k** delineate the compositions of marginal stability, in which some samples were not measurable due to the presence of aggregates. Data are Means ± SD (n≥3).

In FCCS, the confocal volumes defined by the green and red lasers of a confocal microscope are fixed in space, while labelled species diffuse in and out of the overlapping green and red region (Figure 2a). The extent of overlap between the two volumes, determined in separate calibration measurements (SI), is ca. 74.6%. If polyplexes and liposomes do not form a LPNP, they will diffuse independently, and when they enter and leave the confocal volume of the two lasers, they will produce uncorrelated spikes in the two fluorescence signals. This is the case for formulations starting with $\rho_{P:DNA}$=3 polyplexes, in which, discounting for a slight cross-talk of the green to the red channel (that can be corrected), polyplexes and cationic liposomes show unsynchronized spikes in the fluorescence channels (Figure 2b). In contrast, if polyplexes and liposomes form a LPNP, they will diffuse together and when they enter and leave the confocal volume the spikes in the two fluorescence signals will be correlated. This is the case for the formulations starting with $\rho_{P:DNA}$=1.5 polyplexes (Figure 2c), where an almost perfect overlap between the green and red signals is observed for this stretch of time. For the formulations starting with $\rho_{P:DNA}$=1 (Figure 2d), the spikes in the green channel seem to overlap with red spikes, but there are many red spikes that have no overlap with green. This is most likely because a high excess of liposomes is present, producing only red spikes. Overall, even if somewhat qualitative, these observations confirm that LPNPs are forming when the charge is being inverted ($\rho_{P:DNA}$=1 and 1.5), but not when the charge of polyplexes and liposomes has the same sign ($\rho_{P:DNA}$=3).

2.3. FCCS auto- and cross-correlation quantify association between cationic liposomes and polyplexes.

For a more quantitative analysis, the auto- and cross-correlation curves (resulting from time traces) can be examined[43,45,50] (Figures 2e-g). The green and red auto-correlation curves contain information on the fluctuation dynamics of species carrying the green and red labels, respectively. Importantly, the cross-correlation curve results from the correlation between the two signals and therefore only contains information on the fluctuation dynamics of species carrying both labels. The decay time constants of these curves are related with the diffusion coefficients of the species and therefore can be used to extract the particles' size (Table S4). The differences between sizes determined with DLS and FCCS are small, indicating low sample polydispersity.

The amplitude of the correlation curves contain information on the number of each labelled specie, and on the number of species containing both labels[43,49]. Hence, the fraction of polyplexes co-localized with liposomes and consequent LPNP formation can be determined. For the simplified case of: (i) one polyplex associating with one cationic liposome (1:1 stoichiometry) to form one LPNP; (ii) no cross-talk between the two channels; and (iii) no changes in the brightness of the species following the association, the equations relating the amplitudes of the correlation curves with the number of species in the confocal volume become straightforward (Eqs 1a-c)

$$A_G = \left(N_{\mathrm{PP}f} + N_{\mathrm{LPNP}}\right)^{-1} \tag{1a}$$

$$A_R = \left(N_{\mathrm{L}f} + N_{\mathrm{LPNP}}\right)^{-1} \tag{1b}$$

$$A_X = \frac{N_{\mathrm{LPNP}}}{\left(N_{\mathrm{PP}f} + N_{\mathrm{LPNP}}\right) \cdot \left(N_{\mathrm{L}f} + N_{\mathrm{LPNP}}\right)} \tag{1c}$$

Here A_G and A_R are the amplitudes of the green and red auto-correlation, respectively, and A_X is the amplitude of the cross-correlation. $N_{\mathrm{PP}f}$, $N_{\mathrm{L}f}$, and N_{LPNP}, are the average number of free polyplexes, free liposomes and LPNPs in the confocal volumes, respectively. The ratio between A_X and A_R provides a direct measure of the fraction of polyplexes that were converted to LPNPs, according to:

$$A_X/A_R = N_{\mathrm{LPNP}}/\left(N_{\mathrm{PP}f} + N_{\mathrm{LPNP}}\right) \tag{2a}$$

Conversely, the A_X/A_G ratio provides a direct measure of the fraction of cationic liposomes used to make the LPNPs:

$$A_X/A_G = N_{\mathrm{LPNP}}/\left(N_{\mathrm{L}f} + N_{\mathrm{LPNP}}\right) \tag{2b}$$

The approximations above are reasonable since the experimental conditions are such that the cross-talk from the green to the red channel is kept low at ca. 10%, allowing for its correction[59]. The brightnesses of the polyplexes and liposomes also do not change significantly upon association. Finally, the stoichiometry of 1:1 between liposomes and polyplexes is a cruder simplification, but it provides a suitable starting point to analyse the LPNP systems.

To determine the overlap volume correction factor ($V_{crct.}$=74.6%), we performed a controlled experiment using a mixture of single-labelled and double-labelled PEGylated liposomes (Figure S1). A related calibration approach has been recently described by Werner et al.[60] Besides determining V_{crct} this experiment validates the suitability of FCCS to determine colocalization of particles of ca. 100 nm,

comparable to LPNPs. After correcting the cross-talk[59], the A_X used in Eqs. 1-2 is obtained from the measured amplitude of the cross-correlation ($A_{X.meas}$) and $V_{crct.}$ according to:

$$A_X = A_{X.meas.}/V_{crct.} \quad (3)$$

2.4. Liposomes and polyplexes with the same charge do not associate.

Starting with the $\rho_{P:DNA}$=3 system, where we had seen low synchronization between the green and red fluorescence spikes, Figure 2e shows that the amplitude of the cross-correlation curve $A_{X.meas.}$ is much lower than the amplitudes of the autocorrelation curves A_G and A_R. Through Eqs 2, this indicates that indeed there is practically no association between cationic polyplexes ($\rho_{P:DNA}$=3) and cationic liposomes. This lack of association is also illustrated in Figure 2h where the A_X/A_R and A_X/A_G ratios are plotted. Both ratios are close to zero, indicating practically no LPNP formation. As mentioned above, in this $\rho_{P:DNA}$=3 case, the DNA was labelled instead of the polycation, but the absence of cross-correlation still proves the lack of association between polyplexes and liposomes. The results where the polycation is labelled instead of DNA can be seen in Figure S2. Since in this case there are many free labelled polycations in solution, the interpretation of A_X/A_R and A_X/A_G becomes difficult, but the fact that $A_{X.meas.}$ is also here very low corroborates the above interpretation.

In part, these findings were expected. Like-charged polyplexes and liposomes are unlikely to associate, unless there is a strong non-electrostatic interaction between them, or the liposomes replace part of the polycation in the polyplexes. However, some systems composed by cationic polyplexes and cationic liposomes have reported better transfection than the polyplexes alone[61]. It is unclear if in such cases the use of weaker polycations (e.g., polyethyleneimine – PEI) can lead to partial replacement of the polymer by liposomes to form LPNPs. Alternatively, the two particles may not be associating, but the presence of liposomes still boosts the efficacy of polyplexes via a different mechanism. This hypothesis would therefore be worth reinvestigating as it could lead to new insights about transfection mechanisms.

2.5. Oppositely charged liposomes and polyplexes near ρ_{iso} associate strongly

In contrast with the cationic polyplexes, the $\rho_{P:DNA}$=1.5 system shows a much larger $A_{X.meas.}$, comparable to both A_G and A_R indicating strong colocalization (Figure 2f). Since in this case, both labelled species are cationic (polycation with green and liposomes with red), their colocalization indicates strong association between polyplexes and liposomes.

Figure 2i, shows the corrected A_X/A_R and A_X/A_G ratios as a function of the cationic lipid to DNA charge ratio $\rho_{L:DNA}$. It is noticeable that while the mean values present well-defined and robust trends, the individual measurements are significantly noisier, especially A_X/A_R. This occurs because FCCS operates in a quasi-single-particle regime, requiring long measurement times or multiple measurements to reach adequate statistics. Since long measurements are not feasible due to sample drying, shorter measurements were performed with several independently prepared samples, exhibiting a larger variability vanishing when computing the mean. Note also that while the variability of A_X/A_R is significant, the variability of A_X/A_G is much lower. This is expected in a scenario where most polyplexes are converted to LPNPs coexisting with excess liposomes. The apparently noisier nature of the individual measurements is therefore not of concern, as can be also confirmed by the results of LPNPs assembled with 5 and 0% PEG liposomes, which show the same trends—noisy individual A_X/A_R measurements, but robust means with well-defined trends (Figure 3a).

Within the 1:1 liposome to polyplex stoichiometry ratio approximation A_X/A_R is equal to the fraction of polyplexes converted to LPNPs (Eq 2a). It is noticeable that A_X/A_R increases from ca. 1 to 1.42 as $\rho_{L:DNA}$ is increased from 0.5 to 2. This indicates a close-to-full conversion of the polyplexes into LPNPs in detriment of the alternative structures depicted in Figure 1a. The fact that an average A_X/A_R value larger than one is observed for higher $\rho_{L:DNA}$ may indicate that when such large number of liposomes are added to polyplexes, there may be some LPNPs with more than one liposome attached. If full conversion of polyplexes to lipoplexes is assumed, which is reasonable as just discussed, a slightly more advanced, yet approximate, model of one polyplex assembling with n liposomes (1:n stoichiometry) results in n~1.7 for $\rho_{L:DNA}$=2, which indicates that even at the largest $\rho_{L:DNA}$, most LPNPs will be associated with either one or two liposomes, and most liposomes added will be in excess.

Figure 2i also shows the A_X/A_G ratio, which provides directly the fraction of liposomes used to make LPNPs (Eqs 3b). A_X/A_G is greater than one for $\rho_{L:DNA}$=0.5, which suggests that for the smallest $\rho_{L:DNA}$ there may be not enough liposomes to completely coat the polyplexes. This helps explaining why in this composition LPNP solutions are sometimes colloidally unstable. As $\rho_{L:DNA}$ is increased, A_X/A_G starts to steadily decrease, indicating that there is now an excess of liposomes in solution that do not associate with the polyplexes. At the largest $\rho_{L:DNA}$, the fraction of used liposomes is ca. 0.25, showing that for very large $\rho_{L:DNA}$ most liposomes do not associate with polyplexes, which is what one would expect for a 1:n stoichiometry in which n is relatively close to one.

Besides confirming the formation of LPNPs, both A_X/A_R and A_X/A_G together provide a coherent picture of the association between polyplexes and cationic liposomes. The conversion of polyplexes to LPNPs is strongly favoured for $\rho_{P:DNA}$=1.5 and $\rho_{L:DNA}$ >0.5 compositions. As $\rho_{L:DNA}$ increases, the stoichiometry between polyplexes and liposomes increases slightly from 1:1, but most additional liposomes remain free in solution. Importantly, the possible occurrence of alternative structures where DNA is displaced from the polycation does not occur to any significant extent.

2.6. FCCS reveals that the liposome:polyplex number ratio ρ_N is the critical parameter determining stable LPNP formation, not the charge ratio.

In the previous section it became apparent that the ratio between the number of liposomes and polyplexes (ρ_N) is important. This quantity is not straightforward to obtain using common techniques but is easily accessible using FCCS. The total number of polyplexes and liposomes in solution is obtained through A_G^{-1} and A_R^{-1}, respectively (Eqs 1a-b). The A_G/A_R ratio then provides ρ_N. Eqs 1a-b assume a stoichiometry of 1:1 as an approximation, but the fact that the stoichiometry deviates mostly when there are also many free liposomes results in a small error.

Figure 2k shows that for the $\rho_{P:DNA}$=1.5 system, all the samples in the stable region ($\rho_{L:DNA}$≥0.75) have a ρ_N ratio greater than one. Conversely, the samples in the marginally stable region ($\rho_{L:DNA}$=0.5) show a ρ_N slightly below one. This provides a very strong hint that ρ_N≥1 is a critical requirement to obtain robust colloidal stability. By linear interpolation, the boundary where the system transitions from marginal to robust stability (ρ_N=1) is estimated at $\rho_{L:DNA}$=0.63.

We had not anticipated this requirement, but in hindsight, it is not surprising. If the number of liposomes is smaller than the number of polyplexes, some polyplexes will be transformed into cationic LNPNs while some others will remain anionic. Hence, even in a situation of large overall positive charge, if ρ_N<1 the interactions between non-converted anionic polyplexes and cationic LPNPs can lead to aggregation. This also requires, naturally, that each liposome has an absolute charge greater than the polyplexes, and no excess DNA present, or else ρ_N must be larger.

However intuitive, this ρ_N≥1 requirement is a critical insight. The reason why we and others have failed to think of it is because ρ_N is an elusive quantity, difficult to estimate beforehand or determine experimentally. Furthermore, it depends on sample preparation. Hence, ρ_N is not a salient feature in sample preparation that researchers tend to think of, and instead focus on absolute charge ratios. The latter are easier to control experimentally, but less useful in predicting the association between liposomes and polyplexes, since the absolute charges are distributed over a discrete number of particles. FCCS then plays

a crucial role in revealing and highlighting ρ_N by measuring both the number of polyplexes and liposomes simultaneously.

2.7. Polyplexes far from ρ_{iso} are more numerous, requiring more liposomes to form LPNPs.

Overall, $\rho_{P:DNA}$=1 polyplexes show similar trends to the $\rho_{P:DNA}$=1 system (Figures 2g and 2j). Namely, all the polyplexes are converted into LPNPs, as seen from the A_X/A_R ratio, slightly above one, indicating that the average number of liposomes per LPNP is slightly greater than one also. However, there are two important additional points to highlight.

The first is that when significantly away from ρ_{iso}, some of the DNA is expected to remain free in solution, non-complexed[46]. This free DNA also needs to be complexed by the cationic liposomes for the system to become colloidally stable, thus requiring a larger $\rho_{L:DNA}$ ratio. Liposomes complexed with this excess DNA are not expected to be associated with polyplexes, which explains the observation that A_X/A_G is measured at ca. 0.25. However, contrary to the $\rho_{P:DNA}$=1.5 case seen above, where a decreasing A_X/A_G is just indicative of superfluous liposomes, here, these extra liposomes are needed to neutralize free DNA, and almost certainly this indicates coexistence of LPNPs with lipoplexes. This partially explains the much larger $\rho_{L:DNA}$ ratio needed to obtain stability in the $\rho_{P:DNA}$=1 systems.

The second important point is that the number of polyplexes is significantly greater for $\rho_{P:DNA}$=1 than $\rho_{P:DNA}$=1.5. This can be seen by the amplitudes of the green autocorrelation curves in Figures 2f and 2g (~5x greater – recall Eq 2a) and Table S5 (~3.5x greater). The greatest consequence of this larger number of polyplexes is that to ensure the $\rho_N \geq 1$ requirement, the number of liposomes needed to stabilize the system also increases. This, together with the excess of DNA discussed above, helps justifying the much higher $\rho_{L:DNA}$ needed for $\rho_{P:DNA}$=1 LPNPs. The reasons for the much larger number of polyplexes away from the isoelectric point are not obvious. To the best of our knowledge there are no good polymer-complexation models predicting the number of polyplexes. It is also expectable that different polycations complex DNA with different degrees of cooperativity[46]. Since the number of polyplexes formed influences LPNP formation, this further highlights the need to use advanced characterization methods that determine particle concentrations.

2.8. The amount of PEG on liposomes influences the number of liposomes per LPNP.

The findings above are largely reproduced when the 10 mol% PEG liposomes are replaced by 5 and 0 mol% PEG liposomes (Figure 3a). For $\rho_{P:DNA}$=1.5, the three systems behave similarly, with the A_X/A_R ratio slightly above one and gradually increasing with $\rho_{L:DNA}$. As discussed in section 2.5, this indicates close-to-full conversion of polyplexes into LPNPs. Simultaneously, the A_X/A_G ratio decreases steadily

with $\rho_{L:DNA}$, indicating that the fraction of liposomes complexed with polyplexes decreases as more liposomes are added. However, it is also visible that as the PEG amount in the liposomes decreases, both the A_X/A_R and A_X/A_G ratios increase. This is more evident for A_X/A_G, since the A_X/A_R values have larger error bars. Overall, both these ratios indicate that while the average number of liposomes *n* per LPNP is expected to still be relatively small, it increases when the PEGylation degree decreases. Since the PEG coating on liposomes acts as a steric barrier against adsorption of other species, it is not surprising that on average low-PEG liposomes complex more extensively with polyplexes.

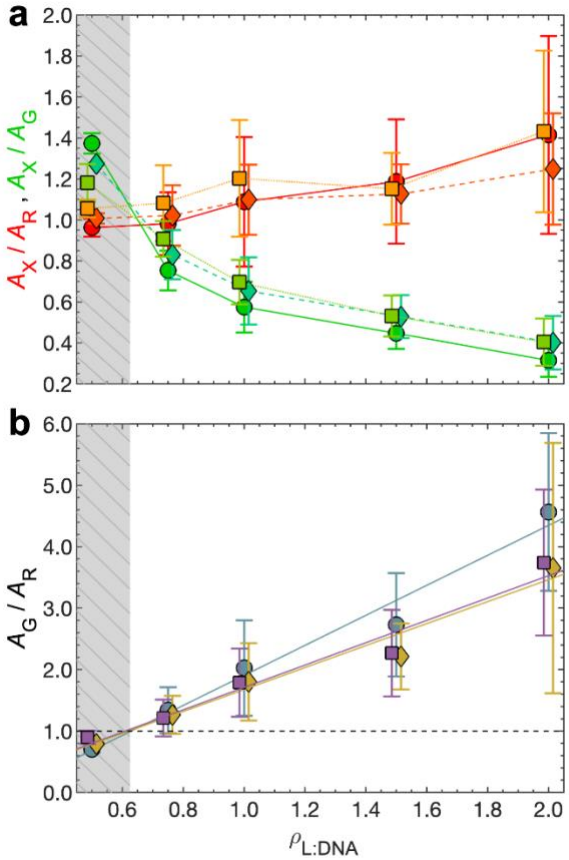

Figure 3. Effect of liposome PEGylation in the assembly of LPNPs. (**a**) A_X/A_R (red-orange symbols) and A_X/A_G (green-blue symbols) ratios for LPNP systems with 0 mol% PEG (squares), 5 mol% PEG (diamonds) and 10 mol% PEG (circles) liposomes. The trends are similar in the three systems, but there is a systematic small increase of the A_X/A_R and A_X/A_G pair for lower degrees of liposome PEGylation. This indicates that the conversion from polyplexes to LPNPs is practically complete for all three systems, but the fraction of used liposomes and average number of liposomes per LPNP increase slightly for lower degrees of liposome PEGylation. (**k**) A_G/A_R ratio for LPNP systems with 0 mol% PEG (squares), 5 mol% PEG (diamonds) and 10 mol% PEG (circles) liposomes. The trends are identical for the three systems. The regions of robust colloidal stability for LPNP formation show ρ_N>1, whereas the regions of marginal stability show ρ_N<1. The boundaries between marginal and robust stability (ρ_N=1) are the same for the three systems ($\rho_{L:DNA}$=0.63). This reinforces that $\rho_N \geq 1$ is a requirement for robust stability. The fact that the linear fits to A_G/A_R have a lower slope for the 0 and 5 mol% PEG systems is caused by the greater deviations to the 1:1 stoichiometry in these systems. Data in **a** and **b** is slightly offset in the horizontal axis for easier visualization. The grey-dashed areas delineate the compositions of marginal stability, in which some samples were not measurable due to the presence of aggregates. Data are Means ± SD (n≥3).

Figure 3b shows the A_G/A_R ratios as a function of $\rho_{L:DNA}$ for the three types of liposomes. As discussed above, the A_G/A_R ratio is equivalent to ρ_N. Like 10 mol% PEG liposomes, also for the lower PEG liposomes we find ρ_N>1 for the stable LPNPs, and ρ_N<1 for the non-stable ones, which reinforces that $\rho_N \geq 1$ is a critical requirement for LPNP colloidal stability. The boundary between marginal and robust stability (ρ_N=1) is similar to the three systems.

Note that similarly to Figures 2i-j, also here the individual measurements appear noisy due to the quasi-single-particle nature of the measurements, but the mean values are robust and follow coherent trends.

2.9. General features of LPNP assembly behaviour and ternary map.

Figure 4 summarises the results and observations of this work in the form of a ternary map of assembly in excess water (given the out-of-equilibrium nature of the system, the map is not strictly a phase diagram).

The first important observation is the lack of formation of LPNPs when starting with positive ($\rho_{P:DNA}$=3) polyplexes (region C on the map). It is unclear whether replacing polylysine with a weaker polycation (e.g., PEI) could result in some displacement of the polymer to allow the deposition of cationic liposomes and enable LPNP formation, but this result should be taken into consideration by formulation scientists as it is not uncommon to design lipid-polymer-gene formulations with similar compositions.

The second important observation is the need to have at least one liposome per polyplex ($\rho_N \geq 1$) to form stable LPNPs. This ensures that every polyplex is enveloped by a liposome, having their negative charge reversed and inhibiting aggregation. This requirement divides region B into two subregions: B1, where aggregation is observed, and B2, where LPNPs stable for at least one week are formed. For $\rho_{P:DNA}$=1.5, the ρ_N = 1 boundary was estimated at $\rho_{L:DNA}$=0.63 (Figure 2k). For $\rho_{P:DNA}$=1, the boundary is difficult to estimate because of the excess DNA, but it lies between $\rho_{L:DNA}$=3 and 5. As an approximation the B1-B2 boundary is thus drawn as a straight line starting in the isoelectric point ($\rho_{P:DNA}$=1.6, $\rho_{L:DNA}$=0), and intersecting the point $\rho_{P:DNA}$=1.5, $\rho_{L:DNA}$=0.63. Besides the approximation, since both the number of polyplexes and liposomes depends both on composition and preparation method, the boundary line is specific to the present work, but is still insightful, and can be used as a point of departure when working with other LPNP systems.

In B2, where stable LPNPs are formed, the conversion of polyplexes to LPNPs is practically full, indicating that neither the polycation nor DNA are displaced by the liposomes. However, the LPNPs still coexist with other (non-competing) species. Along the $\rho_{P:DNA}$=1.5 line LPNPs coexist with excess liposomes, whereas for $\rho_{P:DNA}$=1, they almost certainly coexist with lipoplexes resulting from the complexation of excess DNA. Hence, when investigating biologic activity of LPNP systems, especially if away from ρ_{iso}, the possible coexistence with lipoplexes should be taken into consideration in the elucidation of transfection and therapeutic potential of the formulations.

We have also observed that $\rho_{P:DNA}$=1 systems form ca. 3.5 times more polyplexes than $\rho_{P:DNA}$=1.5 do. This suggests that the polymer-DNA cores contain a smaller number of DNA plasmids in the former than

in the latter, which should be taken into consideration since the number of encapsulated plasmids can be therapeutically relevant[62].

Since the LPNP components chosen for this study are commonly used, we postulate that the general features of assembly observed for this system are similar to other systems containing reasonably strong polyelectrolytes like polylysine and cationic liposomes with monovalent lipids and similar membrane rigidity. Likewise, these generalizations should also extend to: LPNP systems employing cationic polyplexes-anionic liposomes; to LPNPs containing mRNA instead of DNA; and to other composite systems for diverse applications besides gene delivery. If weak polycations (with low ionization degree) are used in the formation of the polyplex cores, or multivalent cationic liposomes, enhanced lipid-DNA interactions in detriment of polycation-DNA could potentially lead to displacement of the polycation and modify the assembly behaviour. Regardless, FCCS would be a crucial aid to quantify the association between the different components and provide valuable insights into the overall assembly behaviour of complex systems.

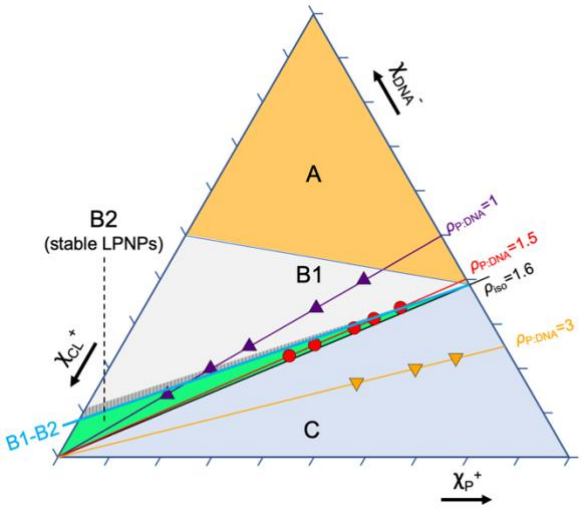

Figure 4. Ternary lipid-polylysine-DNA assembly map in excess water. The three axes represent the charge molar fractions of DNA, polylysine and cationic liposomes. The polylysine concentration is fixed at 7 µg/mL. The map is subdivided in three main regions. Region A encompasses overall negatively charged systems (not investigated). In region B the starting polyplexes are negative but the overall charge is net-positive via addition of cationic liposomes. In sub-region B1 the assemblies are not colloidally-stable whereas in B2 LPNPs stable for at least one week are formed. The B1-B2 boundary between aggregation and stable LPNP formation is set by the liposome:polyplex ratio (ρ_N), which must be $\rho_N \geq 1$ when there is no excess DNA present (see text). The number of liposomes and polyplexes (hence ρ_N) is defined by both the composition and methodology. Within B2, $\rho_{P:DNA}$=1.5 LPNPs coexist with excess cationic liposomes, whereas $\rho_{P:DNA}$=1 LPNPs coexist with lipoplexes. In region C the starting polyplexes are positive (below the ρ_{iso} line), and no LPNP formation was observed after addition of cationic liposomes.

3. CONCLUSIONS

In this work we have unveiled key insights regarding the association of polylysine-DNA polyplex cores with cationic liposome shells to form LPNPs. Firstly, we have shown that this FCCS-based methodology provides an unprecedented amount of information, allowing to rapidly quantify the extent of association between polyplex and liposomes, and map the regions of LPNP formation. Secondly, we have shown that

the interaction between polylysine and DNA is robust, with the polycation not being displaced by liposomes. Hence, the polyplex cores and liposome shells must be oppositely charged to associate and form LPNPs. It is worth noting that if weaker polycations can be displaced by liposomes, the formation of LPNPs by like-charged polyplexes and liposomes may become possible, which would be worth investigating. Thirdly, we showed that the liposome:polyplex number ratio (ρ_N), as opposed to the more common charge ratio, is a critical parameter to predict stable LPNP formation. We find that $\rho_N \geq 1$ is required to ensure that every polyplex is enveloped by a liposome, avoiding the coexistence of oppositely charged species, thus inhibiting aggregation. Furthermore, we have observed important differences in polyplexes depending on $\rho_{P:DNA}$. When further away from the isoelectric point, polyplexes are more numerous and coexist with free DNA, requiring more liposomes to produce LPNPs. Such particles are likely to contain smaller amounts of DNA and coexist with lipoplexes, which should be taken into consideration in formulation design. Finally, Since the chosen LPNP components are common, these observations and FCCS methodology should be applicable to many systems, including other self-assembly composite materials for applications beyond gene delivery.

4. MATERIALS AND METHODS

Materials:

The lipids 1,2-dioleoyl-3-trimethylammonium-propane (DOTAP), 1,2-dioleoyl-sn-glycero-3-phosphocholine (DOPC) and 1,2-distearoyl-sn-glycero-3-phosphoethanolamine-N-[amino(polyethylene glycol)-2000] (DSPE-PEG) solubilized in chloroform were purchased from Avanti Polar Lipids and used as received. Poly-L-lysine solution 0.1 % (w/v) in water was purchased from Sigma-Aldrich. GFP plasmid (pCMV-GFP), obtained through Addgene, was a gift from Connie Cepko (Addgene plasmid #11153)[63]. The dye Atto 488-NHS was purchased from ATTO-TEC GmbH. Texas Red 1,2-Dihexadecanoyl-snGlycero-3-Phosphoethanolamine, Triethylammonium salt (Texas Red-labelled lipid) and the dye YOYO-1 were purchased from ThermoFisher Scientific Inc. All the aqueous solutions were prepared with DNAse-free and RNAse-free MilliQ water.

Characterization techniques:

The different nanostructures obtained in this work were characterized by following techniques: DLS and ζ potential were performed with a SZ-100 device from Horiba, measuring scattering at 173°. TEM of the samples after negative staining with UranyLess© (following the manufacturer´s instructions) was

performed in a JEOL 2100 200kV TEM. FCCS was performed in a confocal microscope LSM780 from Zeiss following a previously described protocol[43], with 5s per measurement and carrying out 40 repeats per sample (excitation laser lines: 488 nm for Atto 488 dye and 561 nm for Texas Red). Laser power was set so that the intensity in the "red" (561 nm) channel was slightly above that in the "green" (488 nm) channel, thus minimizing overestimation of cross-correlation due to cross-talk[59]. FCCS auto- and cross-correlation curves were fitted to a 3D normal diffusion model[64] using QuickFit 3.0 software. After calibrating the FCCS setup employing fluorophores with a known diffusion coefficient[65], the fits obtained for the cross-correlation curves were used to obtain the diffusion coefficient of the LPNPs. Fluorescence intensity time traces were obtained using PyCorrFit software.

Labelling of polylysine with Atto 488 dye:

Polylysine was labelled by reacting the polymer with Atto 488-NHS (ratio 1:100 Atto dye: NH_2 groups in the polymer). After stirring in aqueous solution at room temperature overnight, the labelled polymer was obtained. The purification was performed by size exclusion chromatography using Sephadex G25® stationary phase.

Preparation of LPNPs:

Polyplexes were prepared by mixing aqueous solutions of plasmidic DNA and polylysine at different charge ratios (CR, ratio between positive charges in the polymer to negative charges in the plasmid: 1, 1.5 and 3), and incubating them at room temperature for 30 min in an orbital shaker.

PEGylated cationic liposomes (composition DOTAP/DOPC/DSPE-PEG 80/10/10) were prepared. First, the lipids were mixed in chloroform solution, followed by evaporation of the solvent, rehydration with water and sonication with a tip sonicator at a final total lipid concentration of 4 mM (sonication conditions: 10% amplitude, 1 minute, 50% duty cycle using a Branson Digital Sonifier® 250 Model). Cationic liposomes formulations with the ratios 80/15/5 and 80/20/0 were also prepared.

Finally, both components (polyplex and liposomes) were mixed at different proportions, with a lipid N/DNA P ratio in the range of 0.5-2. A final PLL concentration of 7 µg/mL was fixed for all the prepared samples. The obtained dispersions were characterized by ζ potential and DLS.

For FCCS, the LPNPs were prepared following the same protocol but employing labelled components. Atto 488-labeled PLL was used to prepare the polyplexes, while Texas Red-labelled phospholipid was included in the liposomal formulation (0.2 % total lipid weight). Some samples were also prepared with YOYO 1-labeled DNA and Texas Red-labelled liposomes.

Statistical analysis:

Two-tailed unpaired Students *t* test was employed to test for statistical differences among experimental groups. Differences were considered statistically significant for values of $p<0.05$.

Acknowledgements:

We are grateful to Cyrus Safinya (UCSB), Ulf Olsson (LU) and Paulo Freitas (INL) for useful discussions about this work. This research is supported by Microfluidic Layer-by-layer Assembly of Cationic Liposome - Nucleic Acid Nanoparticles for Gene Delivery project (032520) co-funded by FCT and the ERDF through COMPETE2020. JLP is supported by a post-doctoral fellowship from the Ramón Areces Foundation (reference BEVP30A5827).

5. REFERENCES

(1) Akinc, A.; Maier, M. A.; Manoharan, M.; Fitzgerald, K.; Jayaraman, M.; Barros, S.; Ansell, S.; Du, X.; Hope, M. J.; Madden, T. D.; Mui, B. L.; Semple, S. C.; Tam, Y. K.; Ciufolini, M.; Witzigmann, D.; Kulkarni, J. A.; van der Meel, R.; Cullis, P. R. The Onpattro Story and the Clinical Translation of Nanomedicines Containing Nucleic Acid-Based Drugs. *Nature Nanotechnology* **2019**, *14* (12), 1084–1087. https://doi.org/10.1038/s41565-019-0591-y.

(2) Polack, F. P.; Thomas, S. J.; Kitchin, N.; Absalon, J.; Gurtman, A.; Lockhart, S.; Perez, J. L.; Pérez Marc, G.; Moreira, E. D.; Zerbini, C.; Bailey, R.; Swanson, K. A.; Roychoudhury, S.; Koury, K.; Li, P.; Kalina, W. v.; Cooper, D.; Frenck, R. W.; Hammitt, L. L.; Türeci, Ö.; Nell, H.; Schaefer, A.; Ünal, S.; Tresnan, D. B.; Mather, S.; Dormitzer, P. R.; Şahin, U.; Jansen, K. U.; Gruber, W. C. Safety and Efficacy of the BNT162b2 MRNA Covid-19 Vaccine. *New England Journal of Medicine* **2020**, *383* (27), 2603–2615. https://doi.org/10.1056/NEJMoa2034577.

(3) Baden, L. R.; el Sahly, H. M.; Essink, B.; Kotloff, K.; Frey, S.; Novak, R.; Diemert, D.; Spector, S. A.; Rouphael, N.; Creech, C. B.; McGettigan, J.; Khetan, S.; Segall, N.; Solis, J.; Brosz, A.; Fierro, C.; Schwartz, H.; Neuzil, K.; Corey, L.; Gilbert, P.; Janes, H.; Follmann, D.; Marovich, M.; Mascola, J.; Polakowski, L.; Ledgerwood, J.; Graham, B. S.; Bennett, H.; Pajon, R.; Knightly, C.; Leav, B.; Deng, W.; Zhou, H.; Han, S.; Ivarsson, M.; Miller, J.; Zaks, T. Efficacy and Safety of the MRNA-1273 SARS-CoV-2 Vaccine. *New England Journal of Medicine* **2021**, *384* (5), 403–416. https://doi.org/10.1056/nejmoa2035389.

(4) Kranz, L. M.; Diken, M.; Haas, H.; Kreiter, S.; Loquai, C.; Reuter, K. C.; Meng, M.; Fritz, D.; Vascotto, F.; Hefesha, H.; Grunwitz, C.; Vormehr, M.; Hüsemann, Y.; Selmi, A.; Kuhn, A. N.; Buck, J.; Derhovanessian, E.; Rae, R.; Attig, S.; Diekmann, J.; Jabulowsky, R. A.; Heesch, S.; Hassel, J.; Langguth, P.; Grabbe, S.; Huber, C.; Türeci, Ö.; Sahin, U. Systemic RNA Delivery to Dendritic Cells Exploits Antiviral Defence for Cancer Immunotherapy. *Nature* **2016**, *534* (7607), 396–401. https://doi.org/10.1038/nature18300.

(5) Sahin, U.; Derhovanessian, E.; Miller, M.; Kloke, B. P.; Simon, P.; Löwer, M.; Bukur, V.; Tadmor, A. D.; Luxemburger, U.; Schrörs, B.; Omokoko, T.; Vormehr, M.; Albrecht, C.; Paruzynski, A.; Kuhn, A. N.; Buck, J.; Heesch, S.; Schreeb, K. H.; Müller, F.; Ortseifer, I.; Vogler, I.; Godehardt, E.; Attig, S.; Rae, R.; Breitkreuz, A.; Tolliver, C.; Suchan, M.; Martic, G.; Hohberger, A.; Sorn, P.; Diekmann, J.; Ciesla, J.; Waksmann, O.; Brück, A. K.; Witt, M.; Zillgen, M.; Rothermel, A.; Kasemann, B.; Langer, D.; Bolte, S.;

Diken, M.; Kreiter, S.; Nemecek, R.; Gebhardt, C.; Grabbe, S.; Höller, C.; Utikal, J.; Huber, C.; Loquai, C.; Türeci, Ö. Personalized RNA Mutanome Vaccines Mobilize Poly-Specific Therapeutic Immunity against Cancer. *Nature* **2017**, *547* (7662), 222–226. https://doi.org/10.1038/nature23003.

(6) Pastor, F.; Berraondo, P.; Etxeberria, I.; Frederick, J.; Sahin, U.; Gilboa, E.; Melero, I. An RNA Toolbox for Cancer Immunotherapy. *Nature Reviews Drug Discovery* **2018**, *17* (10), 751–767. https://doi.org/10.1038/nrd.2018.132.

(7) Gillmore, J. D.; Gane, E.; Taubel, J.; Kao, J.; Fontana, M.; Maitland, M. L.; Seitzer, J.; O'Connell, D.; Walsh, K. R.; Wood, K.; Phillips, J.; Xu, Y.; Amaral, A.; Boyd, A. P.; Cehelsky, J. E.; McKee, M. D.; Schiermeier, A.; Harari, O.; Murphy, A.; Kyratsous, C. A.; Zambrowicz, B.; Soltys, R.; Gutstein, D. E.; Leonard, J.; Sepp-Lorenzino, L.; Lebwohl, D. CRISPR-Cas9 In Vivo Gene Editing for Transthyretin Amyloidosis. *New England Journal of Medicine* **2021**, *385* (6), 493–502. https://doi.org/10.1056/NEJMoa2107454.

(8) Lorenzer, C.; Dirin, M.; Winkler, A.-M.; Baumann, V.; Winkler, J. Going beyond the Liver: Progress and Challenges of Targeted Delivery of SiRNA Therapeutics. *Journal of Controlled Release* **2015**, *203*, 1–15. https://doi.org/10.1016/j.jconrel.2015.02.003.

(9) Gupta, A.; Andresen, J. L.; Manan, R. S.; Langer, R. Nucleic Acid Delivery for Therapeutic Applications. *Advanced Drug Delivery Reviews* **2021**, *178*, 113834. https://doi.org/10.1016/j.addr.2021.113834.

(10) Lächelt, U.; Wagner, E. Nucleic Acid Therapeutics Using Polyplexes: A Journey of 50 Years (and Beyond). *Chemical Reviews* **2015**, *115* (19), 11043–11078. https://doi.org/10.1021/cr5006793.

(11) Nakamura, T.; Yamada, Y.; Sato, Y.; Khalil, I. A.; Harashima, H. Innovative Nanotechnologies for Enhancing Nucleic Acids/Gene Therapy: Controlling Intracellular Trafficking to Targeted Biodistribution. *Biomaterials* **2019**, *218* (April), 119329. https://doi.org/10.1016/j.biomaterials.2019.119329.

(12) Degors, I. M. S.; Wang, C.; Rehman, Z. U.; Zuhorn, I. S. Carriers Break Barriers in Drug Delivery: Endocytosis and Endosomal Escape of Gene Delivery Vectors. *Accounts of Chemical Research* **2019**, *52* (7), 1750–1760. https://doi.org/10.1021/acs.accounts.9b00177.

(13) Ewert, K. K.; Scodeller, P.; Simón-Gracia, L.; Steffes, V. M.; Wonder, E. A.; Teesalu, T.; Safinya, C. R. Cationic Liposomes as Vectors for Nucleic Acid and Hydrophobic Drug Therapeutics. *Pharmaceutics* **2021**, *13* (9), 1365. https://doi.org/10.3390/pharmaceutics13091365.

(14) Mitchell, M. J.; Billingsley, M. M.; Haley, R. M.; Wechsler, M. E.; Peppas, N. A.; Langer, R. Engineering Precision Nanoparticles for Drug Delivery. *Nature Reviews Drug Discovery* **2021**, *20* (2), 101–124. https://doi.org/10.1038/s41573-020-0090-8.

(15) Rädler, J. O.; Koltover, I.; Salditt, T.; Safinya, C. R. Structure of DNA-Cationic Liposome Complexes: DNA Intercalation in Multilamellar Membranes in Distinct Interhelical Packing Regimes. *Science* **1997**, *275* (5301), 810–814. https://doi.org/10.1126/science.275.5301.810.

(16) Harries, D.; May, S.; Ben-shaul, A. Counterion Release in Membrane–Biopolymer Interactions. *Soft Matter* **2013**, *9*, 9268–9284. https://doi.org/10.1039/c3sm51419f.

(17) Gaspar, R.; Coelho, F.; Silva, B. F. B. Lipid-Nucleic Acid Complexes: Physicochemical Aspects and Prospects for Cancer Treatment. *Molecules* **2020**, *25*, 5006. https://doi.org/10.3390/molecules25215006.

(18) Buck, J.; Grossen, P.; Cullis, P. R.; Huwyler, J.; Witzigmann, D. Lipid-Based DNA Therapeutics: Hallmarks of Non-Viral Gene Delivery. *ACS Nano* **2019**, *13*, 3754–3782. https://doi.org/10.1021/acsnano.8b07858.

(19) Kim, J.; Eygeris, Y.; Gupta, M.; Sahay, G. Self-Assembled MRNA Vaccines. *Advanced Drug Delivery Reviews* **2021**, *170*, 83–112. https://doi.org/10.1016/j.addr.2020.12.014.

(20) Sebastiani, F.; Yanez Arteta, M.; Lerche, M.; Porcar, L.; Lang, C.; Bragg, R. A.; Elmore, C. S.; Krishnamurthy, V. R.; Russell, R. A.; Darwish, T.; Pichler, H.; Waldie, S.; Moulin, M.; Haertlein, M.; Forsyth, V. T.; Lindfors, L.; Cárdenas, M. Apolipoprotein E Binding Drives Structural and Compositional Rearrangement of MRNA-Containing Lipid Nanoparticles. *ACS Nano* **2021**, acsnano.0c10064. https://doi.org/10.1021/acsnano.0c10064.

(21) Chaudhary, N.; Weissman, D.; Whitehead, K. A. MRNA Vaccines for Infectious Diseases: Principles, Delivery and Clinical Translation. *Nature Reviews Drug Discovery* **2021**, *20* (11), 817–838. https://doi.org/10.1038/s41573-021-00283-5.

(22) Hyodo, M.; Sakurai, Y.; Akita, H.; Harashima, H. "Programmed Packaging" for Gene Delivery. *Journal of Controlled Release* **2014**, *193*, 316–323. https://doi.org/10.1016/j.jconrel.2014.04.023.

(23) Wang, Y.; Huang, L. Composite Nanoparticles for Gene Delivery. In *Advances in Genetics*; Elsevier, 2014; Vol. 88, pp 111–137. https://doi.org/10.1016/B978-0-12-800148-6.00005-5.

(24) Rezaee, M.; Oskuee, R. K.; Nassirli, H.; Malaekeh-Nikouei, B. Progress in the Development of Lipopolyplexes as Efficient Non-Viral Gene Delivery Systems. *Journal of Controlled Release* **2016**, *236*, 1–14. https://doi.org/10.1016/j.jconrel.2016.06.023.

(25) Siewert, C. D.; Haas, H.; Cornet, V.; Nogueira, S. S.; Nawroth, T.; Uebbing, L.; Ziller, A.; Al-Gousous, J.; Radulescu, A.; Schroer, M. A.; Blanchet, C. E.; Svergun, D. I.; Radsak, M. P.; Sahin, U.; Langguth, P. Hybrid Biopolymer and Lipid Nanoparticles with Improved Transfection Efficacy for MRNA. *Cells* **2020**, *9* (9), 2034. https://doi.org/10.3390/cells9092034.

(26) Schäfer, J.; Höbel, S.; Bakowsky, U.; Aigner, A. Liposome–Polyethylenimine Complexes for Enhanced DNA and SiRNA Delivery. *Biomaterials* **2010**, *31* (26), 6892–6900. https://doi.org/10.1016/j.biomaterials.2010.05.043.

(27) Penacho, N.; Rosa, M.; Lindman, B.; Miguel, M. G.; Simões, S.; de Lima, M. C. P. Physicochemical Properties of Transferrin-Associated Lipopolyplexes and Their Role in Biological Activity. *Colloids and Surfaces B: Biointerfaces* **2010**, *76* (1), 207–214. https://doi.org/10.1016/j.colsurfb.2009.10.034.

(28) Caracciolo, G.; Pozzi, D.; Capriotti, A. L.; Marianecci, C.; Carafa, M.; Marchini, C.; Montani, M.; Amici, A.; Amenitsch, H.; Digman, M. A.; Gratton, E.; Sanchez, S. S.; Laganà, A. Factors Determining the Superior Performance of Lipid/DNA/Protammine Nanoparticles over Lipoplexes. *Journal of Medicinal Chemistry* **2011**, *54* (12), 4160–4171. https://doi.org/10.1021/jm200237p.

(29) Persano, S.; Guevara, M. L.; Li, Z.; Mai, J.; Ferrari, M.; Pompa, P. P.; Shen, H. Lipopolyplex Potentiates Anti-Tumor Immunity of MRNA-Based Vaccination. *Biomaterials* **2017**, *125*, 81–89. https://doi.org/10.1016/j.biomaterials.2017.02.019.

(30) van der Jeught, K.; de Koker, S.; Bialkowski, L.; Heirman, C.; Tjok Joe, P.; Perche, F.; Maenhout, S.; Bevers, S.; Broos, K.; Deswarte, K.; Malard, V.; Hammad, H.; Baril, P.; Benvegnu, T.; Jaffrès, P.-A.; Kooijmans, S. A. A.; Schiffelers, R.; Lienenklaus, S.; Midoux, P.; Pichon, C.; Breckpot, K.; Thielemans, K. Dendritic Cell Targeting MRNA Lipopolyplexes Combine Strong Antitumor T-Cell Immunity with Improved Inflammatory Safety. *ACS Nano* **2018**, *12* (10), 9815–9829. https://doi.org/10.1021/acsnano.8b00966.

(31) Lee, R. J.; Huang, L. Folate-Targeted, Anionic Liposome-Entrapped Polylysine-Condensed DNA for Tumor Cell-Specific Gene Transfer. *Journal of Biological Chemistry* **1996**, *271* (14), 8481–8487. https://doi.org/10.1074/jbc.271.14.8481.

(32) Zintchenko, A.; Koňák, Č. Interaction of DNA/Polycation Complexes with Phospholipids: Stabilizing Strategy for Gene Delivery. *Macromolecular Bioscience* **2005**, *5* (12), 1169–1174. https://doi.org/10.1002/mabi.200500159.

(33) Xue, Y.; Feng, J.; Liu, Y.; Che, J.; Bai, G.; Dong, X.; Wu, F.; Jin, T. A Synthetic Carrier of Nucleic Acids Structured as a Neutral Phospholipid Envelope Tightly Assembled on Polyplex Surface. *Advanced Healthcare Materials* **2020**, *9* (6), 1901705. https://doi.org/10.1002/adhm.201901705.

(34) Zhu, X.; Xu, Y.; Solis, L. M.; Tao, W.; Wang, L.; Behrens, C.; Xu, X.; Zhao, L.; Liu, D.; Wu, J.; Zhang, N.; Wistuba, I. I.; Farokhzad, O. C.; Zetter, B. R.; Shi, J. Long-Circulating SiRNA Nanoparticles for Validating Prohibitin1-Targeted Non-Small Cell Lung Cancer Treatment. *Proceedings of the National Academy of Sciences* **2015**, *112* (25), 7779–7784. https://doi.org/10.1073/pnas.1505629112.

(35) Kaczmarek, J. C.; Patel, A. K.; Kauffman, K. J.; Fenton, O. S.; Webber, M. J.; Heartlein, M. W.; DeRosa, F.; Anderson, D. G. Polymer-Lipid Nanoparticles for Systemic Delivery of MRNA to the Lungs. *Angewandte Chemie* **2016**, *128* (44), 14012–14016. https://doi.org/10.1002/ange.201608450.

(36) Kaczmarek, J. C.; Kauffman, K. J.; Fenton, O. S.; Sadtler, K.; Patel, A. K.; Heartlein, M. W.; DeRosa, F.; Anderson, D. G. Optimization of a Degradable Polymer–Lipid Nanoparticle for Potent Systemic Delivery of MRNA to the Lung Endothelium and Immune Cells. *Nano Letters* **2018**, *18* (10), 6449–6454. https://doi.org/10.1021/acs.nanolett.8b02917.

(37) Islam, M. A.; Xu, Y.; Tao, W.; Ubellacker, J. M.; Lim, M.; Aum, D.; Lee, G. Y.; Zhou, K.; Zope, H.; Yu, M.; Cao, W.; Oswald, J. T.; Dinarvand, M.; Mahmoudi, M.; Langer, R.; Kantoff, P. W.; Farokhzad, O. C.; Zetter, B. R.; Shi, J. Restoration of Tumour-Growth Suppression in Vivo via Systemic Nanoparticle-Mediated Delivery of PTEN MRNA. *Nature Biomedical Engineering* **2018**, *2* (11), 850–864. https://doi.org/10.1038/s41551-018-0284-0.

(38) Stadler, C. R.; Bähr-Mahmud, H.; Celik, L.; Hebich, B.; Roth, A. S.; Roth, R. P.; Karikó, K.; Türeci, Ö.; Sahin, U. Elimination of Large Tumors in Mice by MRNA-Encoded Bispecific Antibodies. *Nature Medicine* **2017**, *23* (7), 815–817. https://doi.org/10.1038/nm.4356.

(39) Chapel, J.-P.; Berret, J.-F. Versatile Electrostatic Assembly of Nanoparticles and Polyelectrolytes: Coating, Clustering and Layer-by-Layer Processes. *Current Opinion in Colloid & Interface Science* **2012**, *17* (2), 97–105. https://doi.org/10.1016/j.cocis.2011.08.009.

(40) Zhao, S.; Caruso, F.; Dähne, L.; Decher, G.; de Geest, B. G.; Fan, J.; Feliu, N.; Gogotsi, Y.; Hammond, P. T.; Hersam, M. C.; Khademhosseini, A.; Kotov, N.; Leporatti, S.; Li, Y.; Lisdat, F.; Liz-Marzán, L. M.; Moya, S.; Mulvaney, P.; Rogach, A. L.; Roy, S.; Shchukin, D. G.; Skirtach, A. G.; Stevens, M. M.; Sukhorukov, G. B.; Weiss, P. S.; Yue, Z.; Zhu, D.; Parak, W. J. The Future of Layer-by-Layer Assembly: A Tribute to ACS Nano Associate Editor Helmuth Möhwald. *ACS Nano* **2019**, *13* (6), 6151–6169. https://doi.org/10.1021/acsnano.9b03326.

(41) Yan, J.; Berezhnoy, N. v.; Korolev, N.; Su, C.-J.; Nordenskiöld, L. Structure and Internal Organization of Overcharged Cationic-Lipid/Peptide/DNA Self-Assembly Complexes. *Biochimica et Biophysica Acta (BBA) - Biomembranes* **2012**, *1818* (7), 1794–1800. https://doi.org/10.1016/j.bbamem.2012.03.022.

(42) Zelphati, O.; Uyechi, L. S.; Barron, L. G.; Szoka Jr., F. C. Effect of Serum Components on the Physico-Chemical Properties of Cationic Lipid / Oligonucleotide Complexes and on Their Interactions with Cells. *Biochim. Biophys. Acta* **1998**, *1390*, 119–133. https://doi.org/10.1016/s0005-2760(97)00169-0.

(43) Bacia, K.; Schwille, P. Practical Guidelines for Dual-Color Fluorescence Cross-Correlation Spectroscopy. *Nature Protocols* **2007**, *2* (11), 2842–2856. https://doi.org/10.1038/nprot.2007.410.

(44) Peng, S.; Li, W.; Yao, Y.; Xing, W.; Li, P.; Chen, C. Phase Separation at the Nanoscale Quantified by DcFCCS. *Proceedings of the National Academy of Sciences of the United States of America* **2020**, *117* (44), 27124–27131. https://doi.org/10.1073/pnas.2008447117.

(45) Gómez-Varela, A. I.; Gaspar, R.; Miranda, A.; Assis, J. L.; Valverde, R. R. H. F.; Einicker-Lamas, M.; Silva, B. F. B.; de Beule, P. A. A. Fluorescence Cross-Correlation Spectroscopy as a Valuable Tool to Characterize Cationic Liposome-DNA Nanoparticle Assembly. *Journal of Biophotonics* **2021**, *14* (1), e202000200. https://doi.org/10.1002/jbio.202000200.

(46) Ketola, T.; Hanzlíková, M.; Leppänen, L.; Raviña, M.; Bishop, C. J.; Green, J. J.; Urtti, A.; Lemmetyinen, H.; Yliperttula, M.; Vuorimaa-laukkanen, E. Independent versus Cooperative Binding in Polyethylenimine − DNA. *J. Phys. Chem. B* **2013**, *117*, 10405–10413. https://doi.org/dx.doi.org/10.1021/jp404812a.

(47) Pigeon, L.; Gonçalves, C.; Pichon, C.; Midoux, P. Evidence for Plasmid DNA Exchange after Polyplex Mixing. *Soft Matter* **2016**, *12* (33), 7012–7019. https://doi.org/10.1039/c6sm00575f.

(48) Coelho, F.; Botelho, C.; Paris, J. L.; Marques, E. F.; Silva, B. F. B. Influence of the Media Ionic Strength on the Formation and in Vitro Biological Performance of Polycation-DNA Complexes. *Journal of Molecular Liquids* **2021**, *344*, 117930. https://doi.org/10.1016/j.molliq.2021.117930.

(49) Weidemann, T.; Schwille, P. *Dual-Color Fluorescence Cross-Correlation Spectroscopy with Continuous Laser Excitation in a Confocal Setup*, 1st ed.; Elsevier Inc., 2013; Vol. 518. https://doi.org/10.1016/B978-0-12-388422-0.00003-0.

(50) Kim, S. A.; Heinze, K. G.; Bacia, K.; Waxham, M. N.; Schwille, P. Two-Photon Cross-Correlation Analysis of Intracellular Reactions with Variable Stoichiometry. *Biophysical Journal* **2005**, *88* (6), 4319–4336. https://doi.org/10.1529/biophysj.104.055319.

(51) Kim, S. A.; Heinze, K. G.; Schwille, P. Fluorescence Correlation Spectroscopy in Living Cells. *Nature Methods* **2007**, *4* (11), 963–973. https://doi.org/10.1038/nmeth1104.

(52) Yu, L.; Lei, Y.; Ma, Y.; Liu, M.; Zheng, J.; Dan, D.; Gao, P. A Comprehensive Review of Fluorescence Correlation Spectroscopy. *Frontiers in Physics* **2021**, *9* (April), 644450. https://doi.org/10.3389/fphy.2021.644450.

(53) Berezhna, S.; Schaefer, S.; Heintzmann, R.; Jahnz, M.; Boese, G.; Deniz, A.; Schwille, P. New Effects in Polynucleotide Release from Cationic Lipid Carriers Revealed by Confocal Imaging, Fluorescence Cross-Correlation Spectroscopy and Single Particle Tracking. *Biochimica et Biophysica Acta (BBA) - Biomembranes* **2005**, *1669* (2), 193–207. https://doi.org/10.1016/j.bbamem.2005.02.011.

(54) Schaeffel, D.; Staff, R. H.; Butt, H. J.; Landfester, K.; Crespy, D.; Koynov, K. Fluorescence Correlation Spectroscopy Directly Monitors Coalescence during Nanoparticle Preparation. *Nano Letters* **2012**, *12* (11), 6012–6017. https://doi.org/10.1021/nl303581q.

(55) Cauda, V.; Engelke, H.; Sauer, A.; Arcizet, D.; Bräuchle, C.; Rädler, J.; Bein, T. Colchicine-Loaded Lipid Bilayer-Coated 50 Nm Mesoporous Nanoparticles Efficiently Induce Microtubule Depolymerization upon Cell Uptake. *Nano Letters* **2010**, *10* (7), 2484–2492. https://doi.org/10.1021/nl100991w.

(56) Ma, K.; Zhang, D.; Cong, Y.; Wiesner, U. Elucidating the Mechanism of Silica Nanoparticle PEGylation Processes Using Fluorescence Correlation Spectroscopies. *Chemistry of Materials* **2016**, *28* (5), 1537–1545. https://doi.org/10.1021/acs.chemmater.6b00030.

(57) Wuttke, S.; Braig, S.; Preiß, T.; Zimpel, A.; Sicklinger, J.; Bellomo, C.; Rädler, J. O.; Vollmar, A. M.; Bein, T. MOF Nanoparticles Coated by Lipid Bilayers and Their Uptake by Cancer Cells. *Chemical Communications* **2015**, *51* (87), 15752–15755. https://doi.org/10.1039/c5cc06767g.

(58) Merkle, D.; Lees-Miller, S. P.; Cramb, D. T. Structure and Dynamics of Lipoplex Formation Examined Using Two-Photon Fluorescence Cross-Correlation Spectroscopy. *Biochemistry* **2004**, *43* (23), 7263–7272. https://doi.org/10.1021/bi036133p.

(59) Bacia, K.; Petrášek, Z.; Schwille, P. Correcting for Spectral Cross-Talk in Dual-Color Fluorescence Cross-Correlation Spectroscopy. *ChemPhysChem* **2012**, *13* (5), 1221–1231. https://doi.org/10.1002/cphc.201100801.

(60) Werner, S.; Ebenhan, J.; Haupt, C.; Bacia, K. A Quantitative and Reliable Calibration Standard for Dual-Color Fluorescence Cross-Correlation Spectroscopy. *ChemPhysChem* **2018**, *19* (24), 3436–3444. https://doi.org/10.1002/cphc.201800576.

(61) Penacho, N.; Filipe, A.; Simões, S.; de Lima, M. C. P. Transferrin-Associated Lipoplexes as Gene Delivery Systems: Relevance of Mode of Preparation and Biophysical Properties. *Journal of Membrane Biology* **2008**, *221* (3), 141–152. https://doi.org/10.1007/s00232-008-9092-x.

(62) Zhang, H.; Bussmann, J.; Huhnke, F. H.; Devoldere, J.; Minnaert, A.; Jiskoot, W.; Serwane, F.; Spatz, J.; Röding, M.; de Smedt, S. C.; Braeckmans, K.; Remaut, K. Together Is Better: MRNA Co-Encapsulation in Lipoplexes Is Required to Obtain Ratiometric Co-Delivery and Protein Expression on the Single Cell Level. *Advanced Science* **2021**, *2102072*, 2102072. https://doi.org/10.1002/advs.202102072.

(63) Matsuda, T.; Cepko, C. L. Electroporation and RNA Interference in the Rodent Retina in Vivo and in Vitro. *Proc. Natl. Acad. Sci. U. S. A.* **2004**, *101* (1), 16–22. https://doi.org/10.1073/pnas.2235688100.

(64) Krieger, J. W.; Singh, A. P.; Garbe, C. S.; Wohland, T.; Langowski, J. Dual-Color Fluorescence Cross-Correlation Spectroscopy on a Single Plane Illumination Microscope (SPIM-FCCS). *Optics Express* **2014**, *22* (3), 2358. https://doi.org/10.1364/OE.22.002358.

(65) Kapusta, P. Absolute Diffusion Coefficients: Compilation of Reference Data for FCS Calibration. *Application Note, PicoQuant GmbH* **2010**.